Next Materials 8 (2025) 100902

Contents lists available at ScienceDirect

Next Materials

journal homepage: www.sciencedirect.com/journal/next-materials

Research article

Wetting front dynamic study in Brazilian cements using neutron and X-ray imaging techniques

Higor Rosenberger [a], Márcio Aparecido Bulla Jr [a], Estela Oliari Garcez [c], Nikolay Kardjilov [d], Fabiano Yokaichiya [a], Margareth K.K.D. Franco [b,*]

[a] Universidade Federal do Paraná, UFPR, Brazil
[b] Instituto de Pesquisas Energéticas e Nucleares, IPEN, Brazil
[c] Deakin University, Faculty of Science, Engineering and Built Environment, School of Engineering, Australia
[d] Helmholtz-Zentrum Berlin für Materialienund Energie, HZB, Germany

ARTICLE INFO

Keywords:
Portland cement
X-ray tomography
Neutron radiography

ABSTRACT

Cement-based materials have a complex porous structure that changes over time, and the durability of such materials strongly correlates to the transport of water and ions throughout the pore structure. The type of cement plays an important role on concrete durability. In this study the dynamics of water absorption using three different types of Portland cement: i) high-early strength cement, ii) ground granulated blast furnace slag (GGBFS) blended cement, and iii) pulverized fly ash (PFA) blended cement, at two different curing ages (7 days and 60 days) were investigated. Neutron radiography technique was used for continuous monitoring of the water absorption in cement paste samples, as shown in the film measured by 3 h, showing the radial and longitudinal penetration of water. The evolution of the wetting front was quantified, analyzed and it was observed that the volume of absorbed water presents behavior according to the square root of time based on neutron images for all samples. X-ray tomography technique was used to investigate the differences between the pore structure and volume of pores (air voids). Finally, this article shows that image techniques is a suitable method for analyzing the size, surface and location of single air voids. The combination of the results from X-ray Tomography and Neutron Radiography shows the potential application of these methods for determining air void parameters and demonstrates how microstructure, type of cement and curing time modified the dynamic water absorption. As expect the fastest absorption was observed on the samples cured for 7 days, however results show clear differences between the three types of cement. At the longer curing time, although no significant differences were found in water absorption, there were important differences in the total number and volume of air voids.

1. Introduction

Durability of concrete has been related to its ability to resist the transport of water [1]. Water transports aggressive agents into concrete and the leachate from the concrete interior. Not all of the water in cement paste is transportable. Indeed, different confined water can be transported at different rates. Bordallo et al. [2] define water in cement paste in three categories: (i) bulk water which can be regarded as water in the capillary pores, (ii) confined water which can be envisaged as mostly being water confined in the so called gel pores in the paste and (iii) chemically bound in the reaction products. The gel pores sizes are considered smaller than 100 Å in diameter and an integral part of cement paste. Capillary water (or water in the capillary pores) must be regarded as the main factor in water transport. These pores are of diameters ranging from greater than 1 μm to as small as 100 Å.

At early ages, the transport of water (and chloride ions) in cement paste is dependent on the existence of large interconnected pores – capillary pores. When water is mixed with cement powder (sized between 1 μm – 40 μm) the water is envisaged to form a continuous pore structure, and as the cement hydrates, becomes closed by the hydration products formed as the curing process occurs. The composition of the cement and the presence of supplementary cementitious materials (SCM) also influences the amount and kind of hydrates formed in cementitious systems and thus their porosity. [3–6]. Ultimately, an increase in durability of cementitious systems is also apparent when SCM are blended with Ordinary Portland Cement (OPC) [7–12].

* Corresponding author.
E-mail addresses: margareth_franco@yahoo.com.br, mkfranco@ipen.br (M.K.K.D. Franco).

https://doi.org/10.1016/j.nxmate.2025.100902
Received 12 February 2025; Received in revised form 31 May 2025; Accepted 30 June 2025
Available online 11 July 2025

Table 1
Composition of CPII, CPIV and CPV cement according to the ABNT NBR 16697:2018.

Cement type	Composition (% mass)			
	Clinker + gypsum	Ground Granulated Blast Furnace Slag (GGBFS)	Pulverized Fly Ash (PFA)	Limestone
CPII	94–56	6–34	-	0–10
CPIV	85–45	-	15–50	0–5
CPV	100–95	-	-	0–5

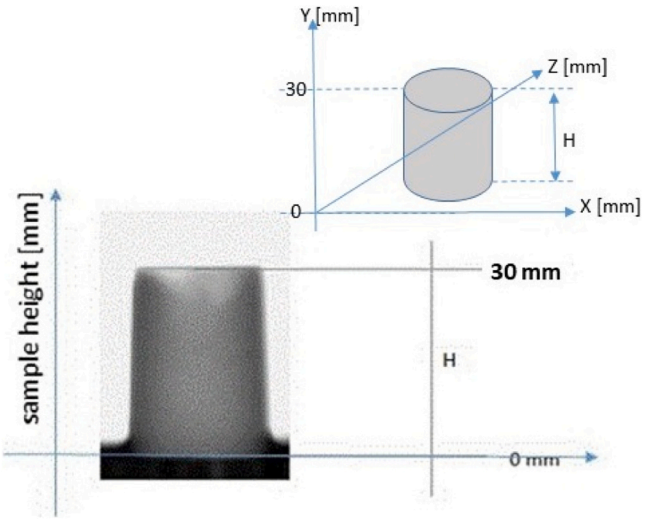

Fig. 1. Neutron image profile of a sample with their longitudinal height, H= Sample height. The darker bottom part of the neutron image refers to water.

SCMs play a dual role during hydration: i) physical effect, referred to as the filler effect, related to changes in the particle spacing and surface availability for nucleation of hydration products; and ii) chemical effect, referred as the pozzolanic effect, which is related to the formation of hydration products and the amorphous silica phases present in SCMs [3, 13]. At early ages, "filler" effects lead to an increased reaction of the clinker (basic material needed to manufacture cement) [1] phases. Reaction of SCMs starts later and is enhanced with pH and temperature. Composition, fineness and the amount of glassy phase play also an important role. The amount of reaction of SCMs in the first days or so is usually negligible and changes in hydration kinetics are dominated by the filler effect [3].

As hydration products fill the capillary pores it becomes more difficult for water to penetrate the cement paste. Generally, the transportation of liquids in porous materials takes place in open pores mainly attributed to permeation and capillary absorption. In most cases, however, cementitious materials are rarely fully saturated during their service life, and capillary water absorption controls the rate of deterioration of structures [14].

Several characterization techniques have been used to study water transport in cement-based materials such as gravimetry[15] nuclear magnetic resonance[16] electrical impedance tomography[17], electrical resistance tomography[18] and electrical impedance spectroscopy [19]. However, the accuracy of these methods is quite limited and therefore the neutron imaging technique proved to be a powerful tool to monitor water transport in cement-based materials [20] observed water imbibition in heat-treated cement mortar samples by neutron radiography showing relationships between microstructure parameters and hydraulic properties of heat-treated mortar.

In this study the dynamics of water imbibition in the samples and air voids distribution was investigated for three different types of Brazilian Portland cement (CPII, CPIV and CPV): i) high-early strength cement, ii) ground granulated blast furnace slag (GGBFS) blended cement, and iii) pulverized fly ash (PFA) blended cement, at two different curing ages - 7 and 60 days. Neutron radiography was employed to quantitatively measure the absorption height and the water content profile in the absorption process, and X-ray tomography technique was used to quantify differences between the structures and distribution of the air voids.

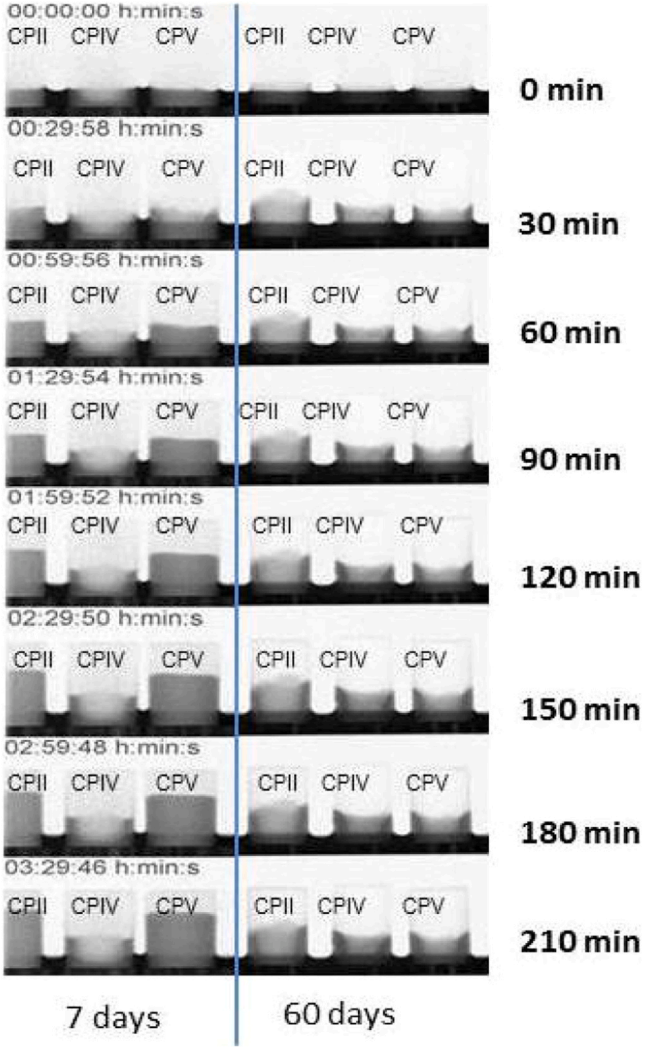

Fig. 2. Image sequence (every 30 min) of samples CPII, CPIV and CPV after 7 (left) and 60 (right) days of curing.

Table 2
Absorption rate (mm per minute).

	CPII		CPIV		CPV	
	7 days	60 days	7 days	60 days	7 days	60 days
Absorption height	22 mm	14 mm	10 mm	10 mm	20 mm	10 mm
Linear absorption rate [mm/min]	0.13	0.07	0.05	0.05	0.10	0.05

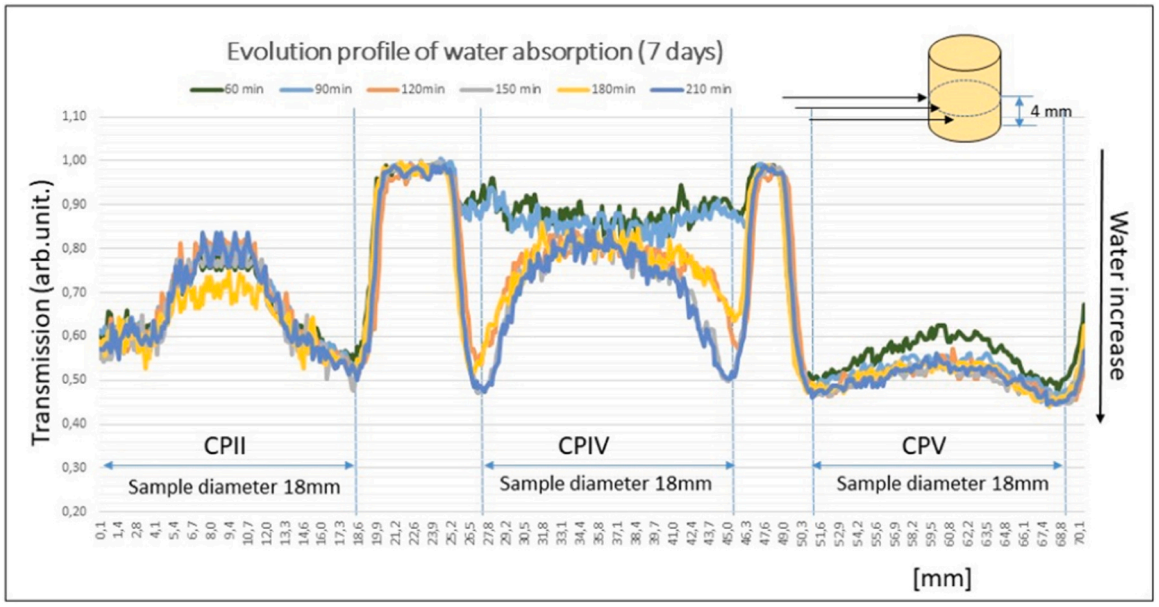

Fig. 3. Time evolution profile of the water absorption in CPII, CPIV e CPV samples (curing time = 7 days, Sample height =14 mm).

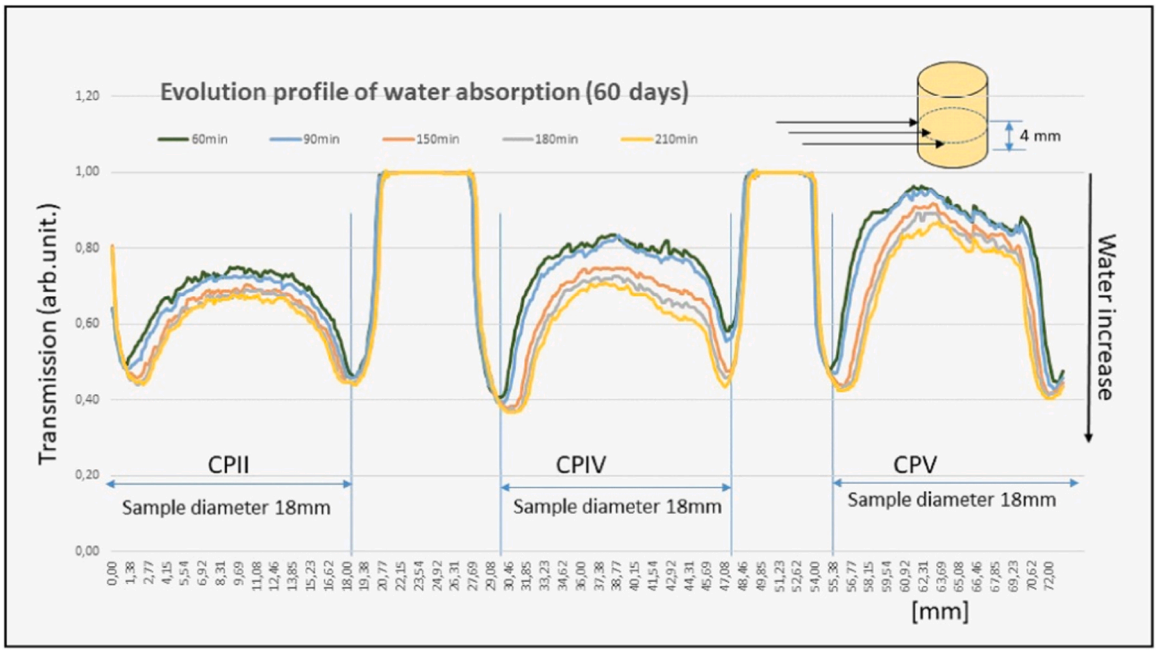

Fig. 4. Time evolution profile of the water absorption in CPII, CPIV e CPV samples (curing time = 60 days, Sample height =14 mm). X axis.

2. Experimental procedure

2.1. Materials

Three types of cement commercially available were used in the preparation of the cement pastes investigated in this study:

- CPII: a blended cement comprising ground granulated blast furnace slag (GGBFS) inter-grounded with ordinary Portland cement (OPC);
- CPIV: a blend of pulverized fly ash (PFA) and OPC; and
- CPV: high-early strength cement, which is a General Purpose cement with finer grains.

The composition of CPII, CPIV and CPV according to the ABNT NBR 16697 [15] is presented in Table 1. The composition of SCM follows ABNT NBR 7215 (1997).

2.2. Sample preparation

All samples were cast in lab environment with controlled temperature (25 ℃). A Hobart blender with 5 L capacity was used for mixing the pastes. Cement pastes were prepared under standard mixing procedures specified in following the ABNT NBR 7215 [16], with water to cement (w/c) ratio of 0.42. Samples were cast in plastic cylindrical molds with 18 mm diameter and 30 mm height. Lids were placed on the top of the molds immediately after casting to ensure appropriate curing. After 24 h, samples were demolded and submerged in water for bath curing until the age of testing, when they were submerged in acetone to stop the

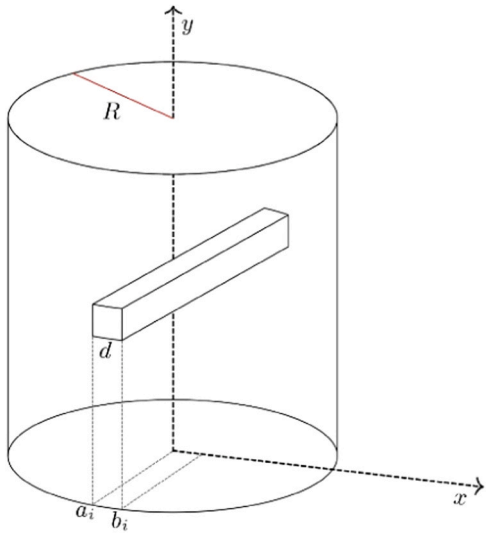

Fig. 5. Example of a pixel volume.

hydration process. The ages of testing (cure days) were 7 and 60 days. Prior to the analysis, the samples were dried at 65°C, during 6 h, in a convection oven to remove remaining water up to a moisture content variation (mass %) lower than 1 %. Fig. 1 shows the profile of the samples with their longitudinal length. Note that the total height of the sample is 30 mm, with 4 mm submerged in distilled water.

For the Neutron radiography measurement, samples CPII, CPIV and CPV with 7 and 60 days of curing were arranged sequentially within a vessel with sufficient distilled water to cover up to the height of 4 mm of the samples. For X-Ray tomography measurements, samples were kept at room temperature and measured immediately after drying.

2.3. Experimental characterization techniques

The water absorption movement in the sample was analyzed by Neutron radiography. The air void structure of the cement paste samples was investigated by X-ray tomography. With this technique, a microstructural analysis and an air void size distribution was obtained. The combination of both techniques enables to correlate the water dynamics and the sample microstructure in order to investigate the behavior of the water absorption as a function of the curing time and type of cement.

The usage of both techniques gathers the resolution power of X-rays with the possibility of direct observation of water using neutrons.

2.3.1. Neutron radiography

Experiments to monitor water absorption were conducted at the installation of the cold neutron radiography light line (CONRAD) at Helmholtz-Zentrum Berlin (HZB). The beam is transmitted through the set of samples and a mirror reflects the image towards the detection system. The detection system consisted of a CCD digital camera facing a LiF/ZnS neutron scintillator screen. The neutron scintillator converts neutron flux into light emission, which is detected by the CCD camera. The set of samples was placed in through-plane orientation to the beam to visualize liquid water across the entire active area. An imaging field-of-view of 200 × 35 mm2 with a pixel size of 26 μm was attained using the imaging set-up developed by Kardjilov et al. [17]. The resolution of the instrument was 250 μm. All the images were corrected using dark current (when the detector is on and the beam is off) and background (when the detector and the beam is on and the sample is out). The monitoring of the water migration process was obtained by the acquisition of data every 31 s for a period of 210 min, which allows the dynamic observation of water absorption.

2.3.2. X-ray tomography

The three-dimensional pore structure of the Portland cements was obtained by laboratorial X-ray microtomography. The measurements

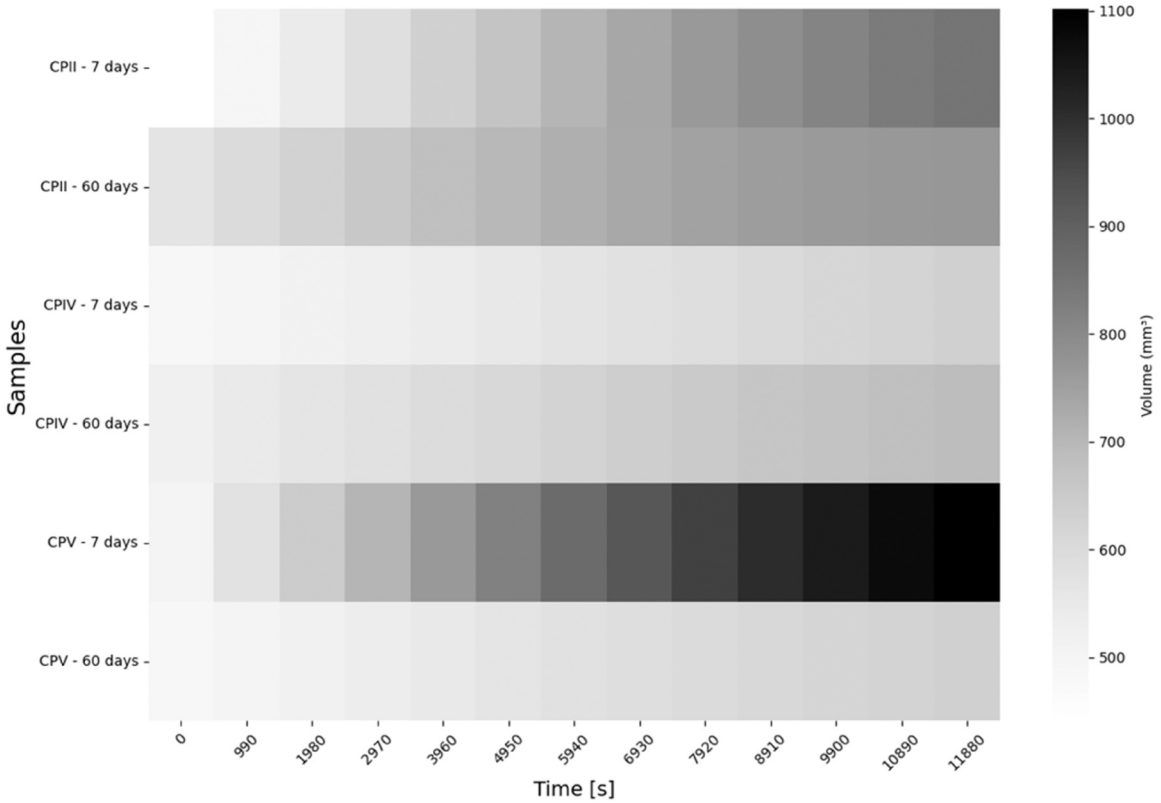

Fig. 6. Heatmap of the volume of water absorbed as a function of time and samples.

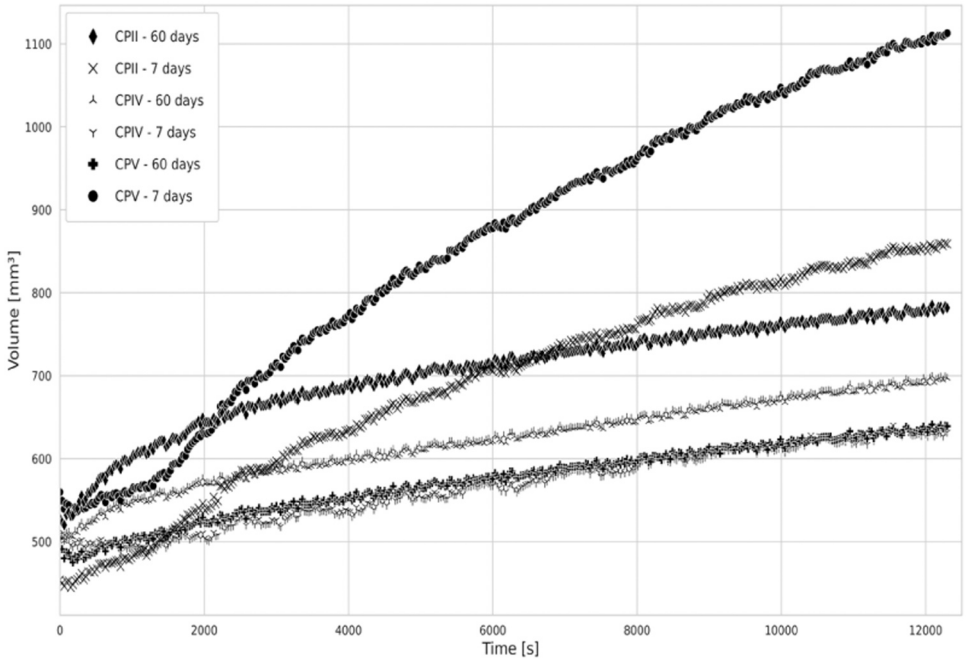

Fig. 7. Water volume as a function of time. It represents the volume of water absorbed by the cylinders as a function of time, providing an overview of the absorption dynamics.

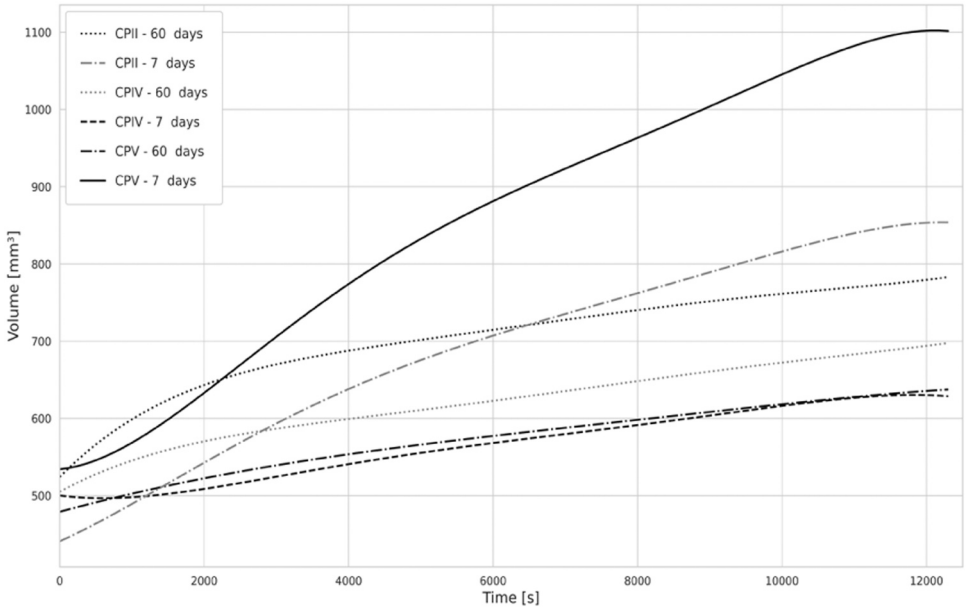

Fig. 8. Adjustment of Volume Polynomials as a Function of Time.

were performed using an imaging setup of the HZB (Helmholtz Centre Berlin for Materials and Energy). This setup consists of a micro-focus 150 kV Hamamatsu X-ray source with a tungsten target and a flat panel detector C7942 (120 ×120 mm, 2240 ×2368 pixel^2, pixel size of 50 μm). A 120 kV filament voltage and a current of 83 μA with an exposure time of 1.4 s per angular projection were used for the scan. The source-object distance was 250 mm and the source-detector distance was 550 mm, achieving thus a magnification factor of 2.2, which reflected in a voxel size of 4027 μm^3. The resolution used was 35 μm. During sample rotation, 1000 radiographic projection images were taken. In order to perform the tomographic reconstruction, we use the commercially available software Octopus V8.6, which was based on a back-projection algorithm with convolution and correction for cone beam.

3. Results and discussions

3.1. Neutron radiography

Fig. 2 shows the water ingress in the CPII, CPIV and CPV samples as a function of time in intervals of 30 min. The images were analyzed based on the intensity of light that passes through the sample. Grey scale represents the presence of water, where the clearest part indicates no presence of water. Higher amounts of water result in darker image.

The visual inspection and analysis of the 2D images allowed a complete identification of the water absorption as a function of type of

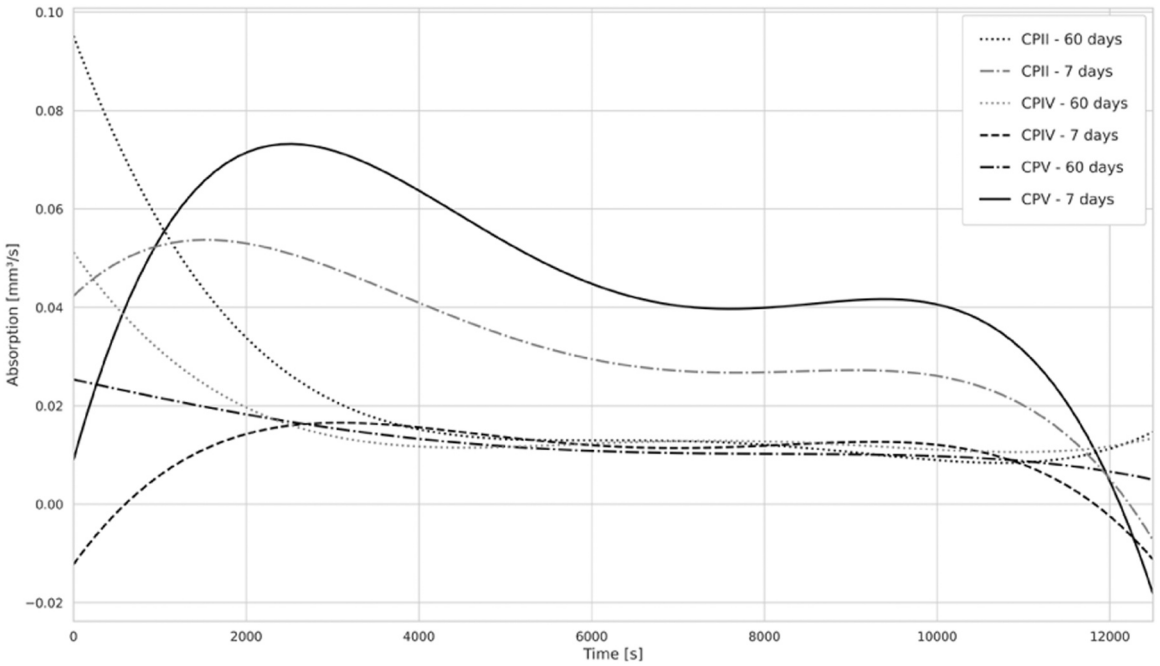

Fig. 9. Rate of change of water volume as a function of time.

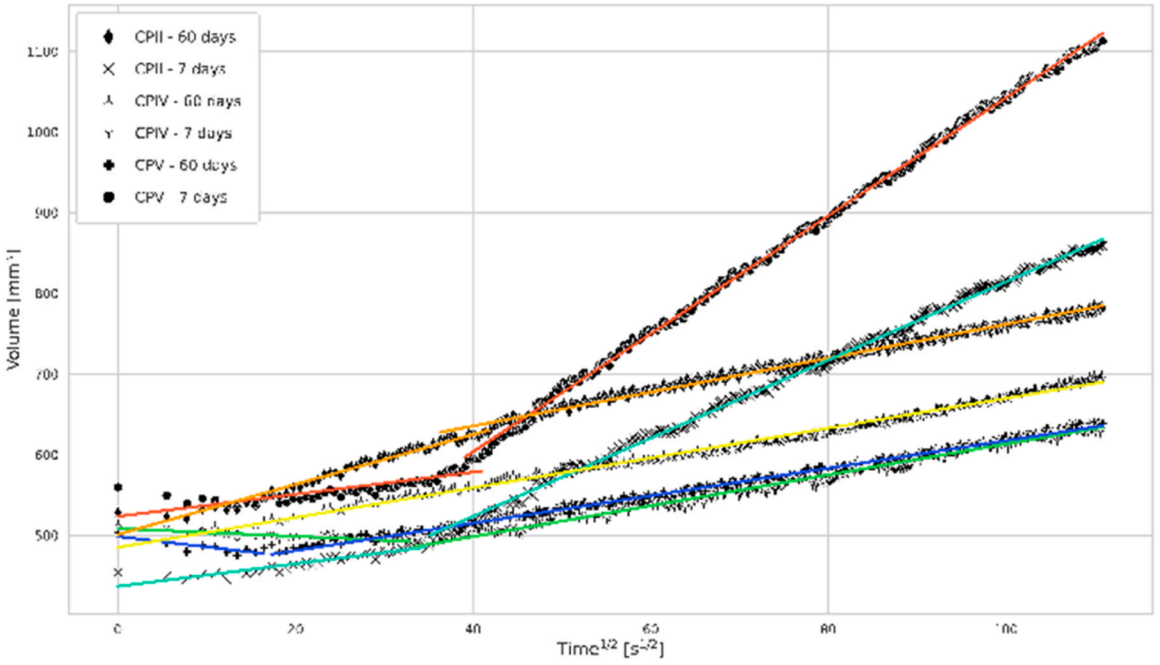

Fig. 10. Linearization: Sample volume as a function of the square root of time. Also fitting of the linearized curves.

cement (CPII, CPIV and CPV) for two different curing time (7 and 60 days).

The absorption rate in the samples (in mm per minute) are compiled in Table 2. After 210 min, it is possible to observe that the samples of CPII and CPV, cured for 7 days, present higher absorption of water. The water absorption profile is equivalent for both samples, while CPIV demonstrates lower absorption height. Both CPII and CPV present lower absorption at 60 days compared to the 7-day cured samples, showing that the curing process decreased the absorption. For the samples cured for 60 days, CPV presents lower absorption than CPII.

The CPIV samples presented equivalent water absorption at 7 and 60 days of curing. CPIV is a blend of pulverized fly ash and OPC, and it is likely that the filler effect has reducing the pore sizes and micro-cracking in the interfacial transition zone [1]. Also the filler effect possibly led to a denser cementitious system and an increased reaction of the cement phases at earlier curing ages. Similar results were found by Aparna et al. [18], where it was demonstrated that rate of water absorption decreases with an increase in fly ash percentage. Kurda et al. [19] also demonstrated that the capillary absorption of concrete decreased when cement was replaced with FA either at early or later ages.

The samples of CPII and CPV presented an absorption rate two times or higher than CPIV at 7 days of cure. However, the water absorption decreases substantially in CPII and CPV samples with 60 days curing. The CPV at 60 days presented permeability equivalent to the CPIV at 60

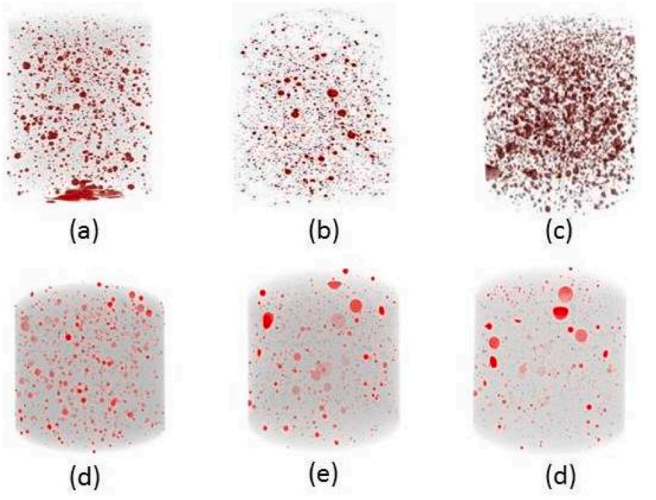

Fig. 11. X-ray tomography of (a) CPII-7 days, (b) CPIV −7days, (c) CPV-7 days and (d) CPII – 60 days, (e) CPIV – 60 days, (d) CPV – 60 days.

days, while the CPII still presented absorption rate 30 % higher than the other cements. These results suggest that the hydration take longer in CPII samples than the other cements. Previous published data [20–22] reported that the pore network of slag cement concretes and mortar were more refined than that observed for OPC cement. In spite of the in-situ analysis of water transport in concrete, mainly using X-ray measurement has already been reported in literature, neutron radiography technique is more suitable to observe water directly [23].

Fig. 3 and Fig. 4 shows the profile of water absorption of each cement type after 7 and 60 days of curing in a fixed position (Sample height = 14 mm). Higher counts mean lower water content. It was possible to observe the water penetration path over 210 min. After 60 min the borders of the samples at 14 mm height are already saturated of water. After 210 min, CPV sample (60 days) is still dry in its core, while the samples CPIV and CPII present higher amount of water in its cores (Figs. 3 and 4).

In order to determine the volume of water absorbed by each sample, we used the profile image of the cylinders obtained through the neutron radiography technique.

Each cylinder has an image with a resolution of 158 × 236 pixels. Considering that the height of the cylinder is 30 mm, each pixel has a dimension of 0.114 mm in both height and width (Fig. 5). The area associated with a pixel is calculated by the expression:

$$A_i = 2\cdot\int_{a_i}^{b_i}\sqrt{R^2 - x^2}dx \tag{1}$$

where the range $[a_i, b_i]$ is constant and equal to d, as shown in Fig. 5. From this expression, the related volume corresponding to a pixel is calculated as:

$$V_i = 2\cdot h\cdot\int_{a_i}^{b_i}\sqrt{R^2 - x^2}dx \tag{2}$$

where R is cylinder radius and h is height of the cylinder. This formulation takes into account the cylindrical geometry of the sample by assigning a specific volume to each pixel, according to its position along the x-axis. This means that the volume corresponding to each pixel is not constant, but varies according to the integral defined by the equation (Eq. 2). Since the image presents 158 pixels in the horizontal direction (corresponding to the diameter of the cylinder), we have 158 distinct integrals — one for each vertical strip. Thus, pixels closer to the center of the cylinder contribute larger volumes than those at the edges, reflecting the geometry of the sample. In other words, the geometric correction is intrinsic to the model used, making any subsequent normalization of the data with respect to the geometry of the sample unnecessary.

The volume of water absorbed corresponding to a pixel is proportional to the gray intensity of the pixel in the image. We define a density scale that ranges from 0 to 1, where 0 represents the total absence of water and 1 represents the maximum volume that a pixel can contain.

To incorporate this gray intensity (Fig. 6), the volume of absorbed water corresponding to a pixel is adjusted by the formula (Eq. 3):

$$V_i = 2\cdot h\cdot i\cdot\int_{a_i}^{b_i}\sqrt{R^2 - x^2}dx \tag{3}$$

where i is the gray intensity of each pixel. Adding the volume of all pixels, we obtain the total volume of water absorbed at a given time t (Eq. 4):

$$V(t) = 2\cdot\sum_{j=1}^{236}\sum_{i=1}^{158} i(t_{i,j})\cdot h_j\cdot\int_{a_i}^{b_i}\sqrt{R^2 - x^2}dx \tag{4}$$

The dynamics of water absorption in the cylinders over time is presented in Fig. 6, which illustrates the variation in the volume of water

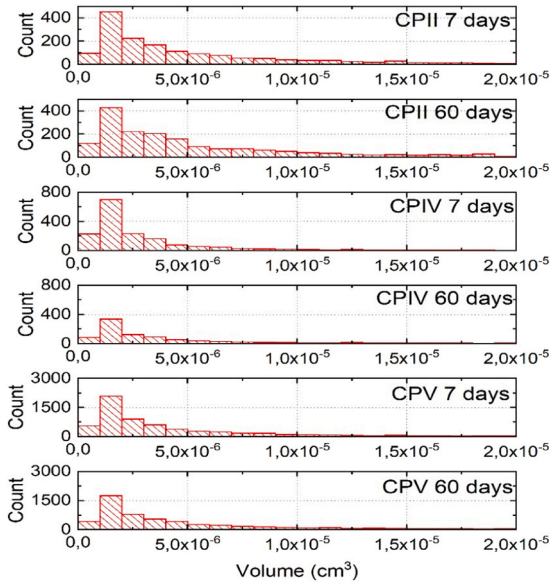

Fig. 12. Distribution curves of the CPII, CPIV and CPV pore volumes at 7 and 60 days of cure.

Table 3
Total number of pores, average pore size, and total volume of voids of samples CPII, CPIV and CPV.

	CP II		CP IV		CP V	
	7 days	60 days	7 days	60 days	7 days	60 days
Number of pores	1670	1798	1517	814	7465	5177
Variation in number of pores	+ 7.7 %		- 46.3 %		−30.6 %	
Average volume [cm^3]	5.78×10^{-6}	5.71×10^{-6}	2.25×10^{-6}	2.78×10^{-6}	3.57×10^{-6}	3.59×10^{-6}
Total volume of voids [cm^3]	0.00965	0.01027	0.00341	0.00226	0.02693	0.01859
Variation in void volume	+ 6.4 %		- 33.7 %		- 31.0 %	

absorbed as a function of time.

Fig. 7 allows the identification of patterns and trends in water absorption, such as periods of rapid absorption or volume stabilization, which may be indicative of saturation processes or changes in absorption dynamics over time.

We perform a curve fitting using polynomials to model water absorption over time. The aim was to obtain a mathematical representation that describes the relationship between the volume of water absorbed and time, allowing a more detailed and predictable analysis of the system behavior.

Fig. 8 shows the fit of the polynomials to the experimental data, the variation in the volume of water absorbed over time and displays the comparison between the experimental data and the adjusted values based on theoretical models, allowing the evaluation of the accuracy of the adjustment and the effectiveness of the model used.

The rate of change was determined based on the difference in the total volume of water absorbed between two consecutive times (Fig. 9), divided by the time interval between these points. This approach allows a detailed analysis of how water absorption changes over time and provides information about the dynamic behavior of the system.

According to the analysis of the experimental data, it was observed that the volume of water absorbed varies linearly with the square root of time. This observation suggests that water absorption is following a nonlinear growth pattern, which can be better represented in terms of the square root of time, as presented in the literature [24].

To corroborate the previous statement, we transformed the time axis to the square root of time and plotted the volume along this new variable (Fig. 9). This transformation was motivated by the realization that the relationship between volume and time was not linear.

The transformation allows for better visualization and analysis of the relationship between water volume and time, simplifying the identification of underlying trends and patterns. It is possible to fit polynomials to the new variable and compare how the model best fits the observed reality.

Below, we present Fig. 10 of the water volume along the square root of time. Through this approach, we seek to verify the linearity of the relationship and obtain a representation of the absorption behavior over time.

We can see from Fig. 10 that all samples with 7 days of curing present two absorption rates, with samples CPII and CPIV having the inflection point before CPV. On the other hand, samples with 60 days of curing present a single absorption rate over time. This suggests that in samples with 7 days, water participates in the hydration reactions, while samples with 60 days of curing are less susceptible to water absorption.

3.2. X-ray tomography

The porosity (air voids) of the different cement samples was investigated using X-ray tomography. Fig. 11 shows the reconstructed tomography images of CPII, CPIV and CPV samples at 7 and 60 days of curing. The images evidence clear differences in the numbers of air voids. Note that due to the resolution of X-ray tomography (50 μm), it is not possible to observe capillary pores and gel pores [25]. The quantitative treatment of the images revealed the average air voids size, the total number of air void and total volume of voids, as presented in Table 3.

Results of tomography showed that the number of pores, obtained using OCTOPUS and VG Studio Max software, in the CPIV and CPV samples decreased with curing time. The reduction in the number of voids in the CPIV sample from 7 to 60 days is 46.3 % while in the CPV sample the observed reduction is 30.6 %. It observed that the porosity in the CPIV sample is 80 % lower than the CPV sample at 7 days and 85 % at 60 days. As expected, these values demonstrate the filler effect in the presence of fly ash in the CPIV at early ages and the increased hydration at later ages.

A reduction in the total volume of voids (33.7 % for CPIV and 31.0 % for CPV) was also observed, which can be clearly verified by the change in the distribution of pore size with curing time presented in Fig. 11. This result could also be observed visually by images showed in Fig. 12.

These histograms show that pores have decreased in size for CPIV and CPV, and remained almost unchanged for CPII over curing time. The CPIV sample presents 8.3 times less volume of voids than CPV at 60 days of curing. These results show the efficiency of the fly ash contained in the CPIV samples both in short and the long term.

The slight increase in the number of pores of CPII samples from 7 days to 60 days of curing can be justified by the presence of blast furnace slag itself and it is not possible to conclude whether there was a real increase or not. From a chemical point of view, when the slag comes in contact with the water it dissolves to a small extent, but a protective film deficient in Ca^{2+} is quickly formed, and inhibits further reaction. Reaction continue if the pH is kept sufficiently high [26]. At 7 days curing, part of the slag may have covered the pores with amorphous material invisible by X-rays. At 60 days, it is possible that the protective film dried and the clusters of grains were caught by the X-rays, which probably represents the number of real pores more precisely.

4. Conclusions

Neutron radiography technique has proved to be a powerful non-destructive technique to study the absorption of the water in cementitious materials as it directly visualizes the position and the water movement in porous cementitious materials. While X-ray tomography provided important insights regarding the structure, distribution and volume of pores.

Results have shown that CPIV samples have equivalent water absorption at 7 and 60 days of curing. CPIV is a blend of pulverized fly ash and OPC, and it is likely that the filler effect has reducing the pores sizes and micro-cracking in the interfacial transition zone.

CPII and CPV have absorption rate two times or higher than CPIV at 7 days of cure. The water absorption decreases substantially in CPII and CPV samples at 60 days curing. At 60-day curing, CPV has permeability equivalent to CPIV, while CPII demonstrated absorption rate 30 % higher than the other cements, suggesting that the hydration reactions take much longer in CPII samples than the other cements.

In this study, a quantitative analysis was performed to show how the experimental results can be used to extract a water transport parameter (dynamic wetting front) in cement pastes. It can be seen from Fig. 10 that the absorption volume is a function of the square root of time. It was noted that in curing times of 7 days, the absorbed water is not only absorbed but also effectively participates in the reactions, resulting in two distinct behaviors of the absorption volume as a function of the square root of time, while in the samples with 60 days, the water is retained and hardly participates in the curing reactions.

Results of tomography showed that the number of pores in the CPIV and CPV samples decreased with curing time. The pore distribution and total volume of pores of CPIV sample clearly demonstrated the filler effect due to the presence of fly ash at early ages and the increased hydration at later ages. The pores have decreased in size for CPIV and CPV, and remained almost unchanged for CPII over curing time.

Thus, the combination of the two techniques associates the quantity of pores (X-ray tomography) with water absorption (neutron radiography), allowing us to understand the dynamics of the wetting front in the cement samples. The CPV samples at both curing times present a greater quantity of pores and consequently a greater water absorption. On the other hand, when comparing the CPII and CPIV samples, although the CPIV sample has more small pores (smaller than 2.10–6 cm3) than the CPII, the water absorption in the CPIV samples is slightly lower because they have a smaller number of large pores (larger than 2.10–6) than the CPII.

Declaration of Competing Interest

The authors declare that they have no known competing financial interests or personal relationships that could have appeared to influence the work reported in this paper.

Acknowledgment

The authors would like to thank HZB staff for the assistance in the tomography measurements.

References

[1] P.K. Mehta, P.J.M. Monteiro, Concrete: Structure, Properties, and Materials, Prentice-Hall International Series in Civil Engineering: Prentice Hall, 1993.
[2] H.N. Bordallo, L.P. Aldridge, A. Desmedt, Water dynamics in hardened ordinary Portland cement paste or concrete: from quasielastic neutron scattering, J. Phys. Chem. B 110 (36) (2006) 17966–17976.
[3] B. Lothenbach, K. Scrivener, R.D. Hooton, Supplementary cementitious materials, Cem. Concr. Res. 41 (12) (2011) 1244–1256.
[4] M.C.G. Juenger, R. Snellings, S.A. Bernal, Supplementary cementitious materials: new sources, characterization, and performance insights, Cem. Concr. Res. 122 (2019) 257–273.
[5] J. Skibsted, R. Snellings, Reactivity of supplementary cementitious materials (SCMs) in cement blends, Cem. Concr. Res. 124 (2019) 105799.
[6] M.D.A. Thomas, et al., The effect of supplementary cementitious materials on chloride binding in hardened cement paste, Cem. Concr. Res. 42 (1) (2012) 1–7.
[7] Y. Ding, et al., The investigation on the workability of fibre cocktail reinforced self-compacting high performance concrete, Constr. Build. Mater. 22 (7) (2008) 1462–1470.
[8] V. Shah, S. Bishnoi, Carbonation resistance of cements containing supplementary cementitious materials and its relation to various parameters of concrete, Constr. Build. Mater. 178 (2018) 219–232.
[9] K. Liu, et al., Effects of combined expansive agents and supplementary cementitious materials on the mechanical properties, shrinkage and chloride penetration of self-compacting concrete, Constr. Build. Mater. 211 (2019) 120–129.
[10] X. Huang, et al., The effect of supplementary cementitious materials on the permeability of chloride in steam cured high-ferrite Portland cement concrete, Constr. Build. Mater. 197 (2019) 99–106.
[11] S. Cheng, et al., Durability and microstructure of coral sand concrete incorporating supplementary cementitious materials, Constr. Build. Mater. 171 (2018) 44–53.
[12] V. Baroghel-Bouny, et al., Easy assessment of durability indicators for service life prediction or quality control of concretes with high volumes of supplementary cementitious materials, Cem. Concr. Compos. 33 (8) (2011) 832–847.
[13] F. Zunino, M. Lopez, Decoupling the physical and chemical effects of supplementary cementitious materials on strength and permeability: a multi-level approach, Cem. Concr. Compos. 65 (2016) 19–28.
[14] J. Zhang, et al., Water distribution modelling of capillary absorption in cementitious materials, Constr. Build. Mater. 216 (2019) 468–475.
[15] TÉCNICAS, A.B.D.N., NBR 16697: Cimento Portland - Requisitos, ABNT: Rio de Janeiro, 2018.
[16] Técnicas, A.Bd.N., ABNT NBR 7215:1996 Cimento Portland - Determinação da resistência à compressão. 1996, ABNT: Rio de Janeiro.
[17] N. Kardjilov, A. Hilger, I. Manke, CONRAD-2: Cold Neutron Tomography and Radiography at BER II (V7), J. LargeScale Res. Facil. JLSRF 2 (A98) (2016).
[18] S. Aparna, D. Sathyan, K.B. Anand, Microstructural and rate of water absorption study on fly-ash incorporated cement mortar, Mater. Today. Proc. 5(11 Part 3 (2018) 23692–23701.
[19] R. Kurda, J. de Brito, J.D. Silvestre, Water absorption and electrical resistivity of concrete with recycled concrete aggregates and fly ash, Cem. Concr. Compos. 95 (2019) 169–182.
[20] Ö. Çakır, F. Aköz, Effect of curing conditions on the mortars with and without GGBFS, Constr. Build. Mater. 22 (3) (2008) 308–314.
[21] K. Wu, et al., Microstructural characterization of ITZ in blended cement concretes and its relation to transport properties, Cem. Concr. Res. 79 (2016) 243–256.
[22] J.M. Ortega, et al., Short-term behavior of slag concretes exposed to a real in situ mediterranean climate environment, Mater. (Basel Switz.) 10 (8) (2017) 915.
[23] P. Trtik, et al., Release of internal curing water from lightweight aggregates in cement paste investigated by neutron and X-ray tomography, Nucl. Instrum. Methods Phys. Res. A 651 (2011) 244–249.
[24] Peng Zhang, et al., Applications of neutron imaging to investigate fundamental aspects of durability of cement-based materials: A review, Cem. Concret Res. 108 (2018) 152–166.
[25] Ivan Zel, et al., Pore segmentation techiques for Low-resolution data: application to the neutron tomography data of cement material, J. Imaging 8 (2022) 242.
[26] H.F.W. Taylor, Cem. Chem. Thomas Telford (1997).